for financial support of the laboratory. Dr. N. Boens and G. Desie are thanked for their contribution in the development of the tcspc analysis program.

References and Notes

(1) De Schryver, F. C.; Moens, L.; Van der Auweraer, M.; Boens, N.; Monnerie, L.; Bokobza, L. *Macromolecules* **1982**, *15*, 64.
(2) Ito, S.; Yamamoto, M.; Nishijima, Y. *Bull. Chem. Soc. Jpn.* **1981**, *54*, 35.
(3) Vandendriessche, J.; Palmans, P.; Toppet, S.; Boens, N.; De Schryver, F. C.; Masuhara, H. *J. Am. Chem. Soc.* **1984**, *106*, 8057.
(4) De Schryver, F. C.; Demeyer, K.; Van der Auweraer, M.; Quanten, E. *Ann. N.Y. Acad. Sci.* **1981**, *366*, 93.
(5) Becker, H. D.; Anderson, K. *J. Org. Chem.* **1982**, *47*, 354.
(6) Semerak, S. N.; Frank, C. W. *Adv. Polym. Sci.* **1984**, *54*, 31.
(7) De Schryver, F. C.; Boens, N.; Put, J. *Adv. Photochem.* **1977**, *10*, 359.
(8) Collart, P.; Toppet, S.; Zhou, Q. F.; Boens, N.; De Schryver, F. C. *Macromolecules* **1985**, *18*, 1026.
(9) Zachariasse, K. A.; Busse, R.; Duveneck, G.; Kuhnle, W. *J. Photochem.* **1985**, *28*, 237.
(10) De Schryver, F. C.; Vandendriessche, J.; Demeyer, K.; Collart, P.; Boens, N. *Polym. Photochem.* **1985**, *6*, 215.
(11) Vollmann, H.; Becker, H.; Correll, M.; Streeck, H.; *Justus Liebigs Ann. Chem.* **1937**, *531*, 1.
(12) Nakasuji, K.; Akiyama, S.; Nakagawa, M. *Bull. Chem. Soc. Jpn.* **1972**, *45*, 875.
(13) Desie, G.; Boens, N.; Van den Zegel, M.; De Schryver, F. C. *Anal. Chim. Acta* **1985**, *170*, 45.
(14) Van den Zegel, M.; Boens, N.; Daems, D.; De Schryver, F. C. *Chem. Phys.* **1986**, *101*, 311.
(15) Bovey, F. A.; Hood, F. P., III; Anderson, E. W.; Snyder, L. C. *J. Chem. Phys.* **1965**, *42*, 3900.
(16) Ito, S.; Yamamoto, M.; Nishijima, Y. *Bull. Chem. Soc. Jpn.* **1982**, *55*, 363.
(17) Birks, J. B.; Dyson, D. J.; Munro, I. H. *Proc. R. Soc. London* **1963**, *275*, 36.
(18) Gorin, S.; Monnerie, L. *J. Chim. Phys. Physicochim. Biol.* **1970**, *67*, 869.
(19) Froelich, B.; Noel, C.; Jasse, B.; Monnerie, L. *Chem. Phys. Lett.* **1976**, *44*, 159.
(20) De Schryver, F. C.; Collart, P.; Vandendriessche, J.; Goedeweeck, R.; Swinnen, A. M.; Van der Auweraer, M. *Acc. Chem. Res.*, in press.

Plasticization of Poly(butyral-*co*-vinyl alcohol)

Jacob Schaefer,*† Joel R. Garbow,‡ and E. O. Stejskal§

Physical Sciences Center, Monsanto Company, St. Louis, Missouri 63167

J. A. Lefelar

Monsanto Chemical Company, Springfield, Massachusetts 01151.
Received October 10, 1986

ABSTRACT: The partitioning of polymer and plasticizer into soft and hard regions for mixtures of poly(butyral-*co*-vinyl alcohol) and dihexyl adipate has been determined by magic-angle-spinning ^{13}C NMR. The soft regions are detected by Fourier-transform techniques with scalar decoupling and the hard regions by cross-polarization with dipolar decoupling. This two-phase character of plasticized polybutyral is also observed in small-angle neutron scattering experiments in which integrated scattering intensity increases linearly with plasticizer concentration. We attribute the soft regions to liquid plasticizer containing mobile polymer and the hard regions to solid polymer associated with partially immobilized plasticizer. There is no chemical exchange between hard and soft regions on a 1-s time scale. The frequencies but not the amplitudes of cooperative main-chain motions of the polymer in the hard regions are influenced by interactions with the soft regions. This result is incorporated into a two-phase domain model that is used to rationalize the macroscopic stress–relaxation properties of these plasticized polymers.

Introduction

A plasticizer is a liquid that is soluble in a glassy polymer, lowers the glass transition of the polymer, and reduces its modulus.[1] Mechanisms of plasticization are not detailed, but the conventional model envisions a homogenous, dynamic interaction between polymer and diluent, resulting in reduced chain-chain interactions, reduced local viscosity, and increased microscopic chain mobility.[2] This is especially true at low diluent concentration. At higher concentrations, depending on polymer–diluent compatibility, phase separation may occur, with diluent association apparent in mechanical and dielectrical response.[3] The system is now heterogeneous, with variations in the degree of plasticization of the polymer depending upon local conformation, or, for copolymers, composition.

We have examined the plasticization of poly(butyral-*co*-vinyl alcohol) (78 wt % polybutyral, known commercially as Butvar) by dihexyl adipate using Fourier-transform (FT) ^{13}C NMR, cross-polarization (CP) magic-angle-spinning (MAS) ^{13}C NMR, and small-angle neutron scattering (SANS). The results are not consistent with the conventional picture of plasticization. Even at low levels of plasticizer, this system is heterogeneous, consisting of microscopic soft regions of liquid diluent containing dissolved polymer, embedded in a hard matrix of solid polymer associated with immobilized plasticizer. The partitioning between the two types of regions persists with increasing levels of plasticizer. We have found that mechanical, thermal, and chain-dynamics measurements can be described in terms of the interactions within and between these soft and hard regions.

Experiments

Magic-Angle Spinning. Carbon-13 MAS spectra and relaxation measurements were made on a spectrometer built around a 12-in. iron magnet operating at a proton Larmor frequency of 60 MHz.[5] The magic-angle rotor (Figure 1) is of the double-bearing type,[6] in which a cylindrical sample chamber is supported between two cylindrical gas journal bearings.[7] The rotor is held in position by a gas thrust bearing at one end, perpendicular to the rotation axis. The rotor is driven by an array of tangential

† Present address: Department of Chemistry, Washington University, St. Louis, MO 63130.
‡ Present address: Monsanto Company, Life Sciences NMR Center, Chesterfield, MO 63198.
§ Present address: Department of Chemistry, North Carolina State University, Box 8204, Raleigh, NC 27695.

0024-9297/87/2220-1271$01.50/0

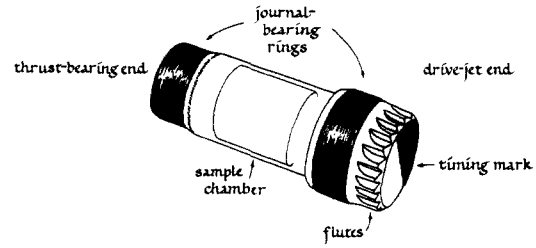

Figure 1. Double-bearing magic-angle rotor.

gas jets impinging on flutes at the other end of the rotor.

The sample chamber is 9.65 mm long by 8.76 mm in diameter (volume of 0.58 cm^3). The radio-frequency coil is free standing and consists of six turns of gold-plated copper ribbon. The coil is 14 mm long with a 10.5-mm inside diameter. The sample is short enough to maintain H_1 homogeneity. The radial distance between the outside surface of the rotor and the inside surface of the coil is 0.87 mm, which provides a good filling factor and long rotor life.

The rotor is made entirely of Kel-F except for the journal-bearing areas, which are protected and stabilized with cylindrical bands of Vespel SP-21 graphite-filled polyimide (trademark of E.I. du Pont de Nemours and Co.). For greater dimensional stability, the Kel-F is roughly shaped and then annealed (115 °C for 16 h in an inert atmosphere) before being cut to the final dimensions. The rotor has been tested to 2.2 kHz without signs of distortion or deterioration. It is normally operated at 1859 Hz (period of 538 μs). Fiber optics and a timing mark on the rotor are used to measure the rotor speed. A voltage-variable valve in the drive-air supply is used to control the rotor period to better than ±0.5 μs.

The journal bearing near the thrust-bearing end is smaller in diameter than the sample-chamber outside diameter, which, in turn, is smaller than the journal-bearing diameter at the drive-jet end. This arrangement provides for strong closures at both ends of the sample chamber and thin walls in the coil area. Since the two journal bearings have different gas demands, the stator is supplied with four independent air supplies: one for the thrust bearing, one for the drive jets, and two for the journal bearings. (Alternatively, a single journal-bearing air supply can be used with this rotor if the radial clearances of the two journal bearings are made unequal.) The other double-bearing rotors in our laboratory (including the one used to obtain the 50-MHz spectrum shown in this paper) have journal bearing of the same diameter and require only a single journal-bearing air supply.[8]

NMR Signal Intensities. Intensities of CP MAS spectra were adjusted for variations in rotating-frame proton and proton–carbon relaxation rates by systematic variation of the contact time.[9] Most CP MAS spectra were obtained under matched Hartmann–Hahn conditions with a 2-ms contact at 50 kHz. Rotating-frame relaxation rates were obtained by standard procedures.[10] FT MAS ^{13}C NMR spectra were fully relaxed.

Carbon Dipolar Tensors. Carbon dipolar tensors were characterized by dipolar rotational spin-echo ^{13}C NMR at 15.1 MHz with magic-angle spinning[11] at 1859 Hz. This is a two-dimensional experiment[12-16] in which, during the additional time dimension, carbon magnetization is allowed to evolve under the influence of C–H coupling while H–H coupling is suppressed by homonuclear multiple-pulse semiwindowless MREV-8 decoupling.[17-19] The 33.6-μs cycle time for the homonuclear decoupling pulse sequence results in decoupling of proton–proton interactions as large as 60 kHz (1/16.8 μs). For singly protonated carbons whose resonances are well resolved in the chemical-shift dimension, a Fourier transform of the intensity at the peak maximum vs. evolution time yields a dipolar spectrum consisting of a ^{13}C–^{1}H Pake doublet, scaled by the MREV-8 decoupling, and broken up into sidebands by the magic-angle spinning. Molecular motion modifies this pattern just as it does quadrupolar line shapes.[20]

Carbon dipolar-tensor simulations were performed by the methods developed by Herzfeld and Berger.[21] Calculations of tensors partially collapsed by restricted molecular motion were performed by assuming that the motion was fast compared to the dipolar interactions. Formulas for tensor components under various types of restricted motions (and compatible with the Herzfeld and Berger analysis) are given in the appendix to ref 22.

Table I
Composition and Elements of Molecular Weight Distribution for Three Butvar Resins

polymer	poly(vinyl alcohol) content, wt %	M_w/M_n	M_z/M_n	M_{z+1}/M_n
A	18	2.4	6.9	18.6
B	18	2.3	7.3	22.2
C	19	2.3	6.0	20.3

Small-Angle Neutron Scattering. SANS experiments were performed at the Oak Ridge National Laboratory High-Flux Isotope Reactor using the 30-m spectrometer. Thermal neutrons with a wavelength of 4.75 Å were used. Scattering patterns were recorded with a two-dimensional position-sensitive detector located 18 m from the sample. Momentum transfer was sampled in the regime 0.003 $Å^{-1} < k < 0.030$ $Å^{-1}$ ($k = 4 \sin(\theta/\lambda)$ and θ is half the scattering angle). Scattering patterns were recovered as two-dimensional contour plots. Since the scattering was isotropic, the coherent differential scattering cross section per unit solid angle per unit sample volume, $d\sigma/d\Omega$, was averaged radially as a function of scattering vector, corrected for instrument background and sensitivity, and stored as absolute intensity, I_k, vs. scattering vector, k.[23] A correction for coherent- and incoherent-background scattering was made before data analysis was begun.[24]

The corrected scattering profiles were fit to two scattering models. The first model used spheres of radius R and scattering-length density ρ.[25] The second model uses shell-core spheres of inner radius R_1 and scattering-length density ρ_1 and outer radius R_2 and scattering-length density ρ_2.[25] The scattering invariant, Q, which is proportional to the mean-square fluctuation in scattering power, was calculated from $Q = \int I_k k^2 \, dk$.[26]

Materials. Butvar is a commerical product of Monsanto Chemical Co. (Indian Orchard, MA). This resin is a copolymer containing primarily vinyl alcohol and butyral comonomers, in an approximately 20/80 ratio, by weight. Details of the acetylation of the starting poly(vinyl alcohol) determine physical properties. Saflex, a clear, uniform material, is the Monsanto commercial product made from the plasticization of Butvar by dihexyl adipate.

Polymer Characterization. Molecular weight distributions of three Butvar resins (Table I) were determined by gel permeation chromatography using two detectors: the first, a low-angle laser light scattering detector (for absolute molecular weights) and the other a differential refractive index detector (for concentration determinations). Thermal conductivity at 25 °C was determined by a comparative method involving calibrated thermocouples placed between reference standards of geometry identical with that of the analytical sample. The samples were 2.5 cm in diameter by 0.67–1.5 cm thick.

Results

NMR Line Assignments. The 15.1-MHz dipolar-decoupled CP MAS ^{13}C NMR spectrum of a solid Butvar resin (polymer A, Table I) is well enough resolved to allow an identication of all the major structural carbons (Figure 2). The configuration of the butyral anomeric carbon is evident by resolution of line 6 into α and β components. This is similar to the resolution of the anomeric carbon resonance of polysaccharides.[27] Under magic-angle-spinning conditions, the scalar-decoupled FT MAS spectrum of Butvar resins shows a broad unresolved resonance, centered about 60 ppm, and a somewhat sharper feature, near 20 ppm (Figure 3, upper left). The latter arises from the methyl carbons of the solid resin. With no dipolar decoupling, the other protonated carbon lines are broad.

In the presence of dihexyl adipate plasticizer, the dipolar-decoupled CP MAS spectrum is reduced in total integrated intensity and broadened (Figure 3, lower right). In addition, there is significant new intensity near 25 and 60 ppm arising from the protonated carbons of the plas-

Table II
Partitioning of Polymer and Dihexyl Adipate between Hard and Soft Regions for Three Plasticized Butvar Resins

polymer	plasticizer concn, phr	integral FT intensity of resin[a]	integral CP intensity of resin[b]	sum of resin FT and CP intensities: obsd	sum of resin FT and CP intensities: theor	β/α[c]	% plasticizer as solid[d]	% resin in soln[e]
A	0	17	83	100	100	0.22		0
	10	15	80	95	91	0.25	60	1
	20	20	50	70	85	0.26	40	19
	32	25	40	65	76	0.38	25	31
B	32	20	40	60	76	0.61	44	25
C	32	16	25	41	76	0.50	32	34

[a] Area of broad line centered at 60 ppm; spectrum obtained with scalar decoupling and magic-angle spinning. [b] Total area of CP spectrum, less immobilized plasticizer contribution centered at 25 ppm; spectrum obtained with dipolar decoupling and magic-angle spinning. [c] Ratio of peak heights of the pair of lines near 100 ppm in CP MAS spectra. [d] From ratio of CP and FT intensities at 25 ppm. [e] From intensity of broad line in FT spectrum of plasticized resin, less intensity of broad line in FT spectrum of resin alone, compared to CP intensity of plasticized resin, less immobilized plasticizer contribution centered at 25 ppm.

Table III
Mechanical, Thermal, and NMR Relaxation Properties of Three Plasticized Butvar Resins

polymer	plasticizer concn, phr	relaxn of 103 ppm line in CP MAS spectrum: $\langle T_{1\rho}(C)\rangle$,[a] ms	$\langle T_1(C)\rangle$,[b] s	$\langle T_{1\rho}(H)\rangle$,[c] ms	dipolar echo refocusing, %	modulus[d] $\times 10^5$, dyn/cm^2	thermal conductivity,[f] W/mK	T_g,[g] °C
A	0	21	3	9	64	30[e]	0.236	80
	10	17	3	7	63	16	0.275	60
	20	14	2	5	57	8.6	0.254	40
	32	7	3	4	44	5.6	0.272	29
B	32	4	1	2	33	1.5	0.265	29
C	32	4	0.5	2	48	7.0	0.265	29

[a] $H_1(C)$ = 37 kHz; least-squares fit to the observed decay between 0.05 and 1.00 ms after turnoff of $H_1(H)$. See ref 10. [b] $H_0(C)$ = 15.1 MHz. [c] $H_1(H)$ = 50 kHz. [d] From stress relaxation after 10^4 s at 60 °C under 40% torsional shear strain. [e] From extrapolation of temperature and plasticizer concentration dependences. [f] At 25 °C. [g] From Rheovibron mechanical loss spectroscopy at 1 Hz.

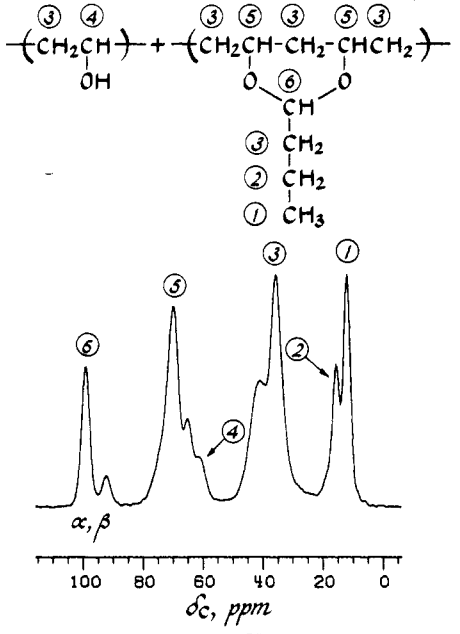

Figure 2. 15.1-MHz CP MAS ^{13}C NMR spectrum and line assignments for a Butvar resin (polymer A).

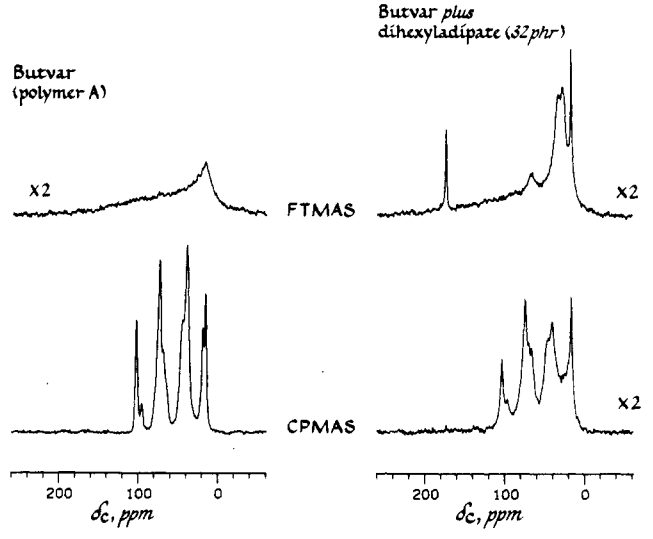

Figure 3. 15.1-MHz dipolar-decoupled CP MAS and scalar-decoupled FT MAS ^{13}C NMR spectra of a Butvar resin (polymer A) with (right) and without (left) plasticizer at 32 phr. The vertical scales have been adjusted to take into account sample size, number of scans, and cross-polarization, rotating-frame, and nuclear Overhauser relaxation parameters.

ticizer. This contribution is not critically sensitive to the contact time, so it arises from dipolar rather than scalar coupling.

The FT MAS spectrum of the plasticized resin is dominated by signals arising from the dihexyl adipate, but the intensity of the broad unresolved resonance centered at 60 ppm is increased in intensity relative to that of the CP MAS spectrum of the same plasticized resin (Figure 3, upper and lower right). The relative intensities of FT MAS and CP MAS spectra are presented in Table II for three plasticized Butvar resins (polymers A, B, and C), one as a function of plasticizer concentration.

The physical properties of the plasticized Butvars were not affected by the magic-angle spinning. The plasticizer remained dispersed and the observed spectra did not change significantly with time, even after several weeks of spinning.

Chain Dynamics and Relaxation Rates. Microscopic chain dynamics of the resin of the three fully plasticized Butvar polymers are monitored by T_1s and $T_{1\rho}$s of the CP MAS butyral carbon line at 103 ppm (Table III, columns 3–5, rows 4–6). The dynamics of polymers B and C are

Table IV
Radio-Frequency Field Dependence of Carbon-13 Rotating-Frame Relaxation Times for a Butvar Resin with and without Plasticizer

polymer	H_1(C), kHz	$\langle T_{1\rho}(C)\rangle$, ms 103 ppm[b]	75 ppm	35 ppm	11 ppm
A (0 phr plasticizer)	60	36	34	21	39
	50	30	28	14	34
	44	35	27	12	40
	37	21	17	7	26
A (32 phr plasticizer)	60	7	5	3	9
	50	7	6	4	10
	44	6	5	3	7
	37	7	5	3	8

[a] Least-squares fit to the observed decay between 0.05 and 1.00 ms after turnoff of H_1(H). See ref 10. [b] See Figure 2.

similar to one another but different from that of polymer A. (The $\langle T_{1\rho}(C)\rangle$'s of the unplasticized resins are also different. For example, the $\langle T_{1\rho}(C)\rangle$ at 50 kHz of the 103 ppm line of polymer B is about 50% longer than that of polymer A.) The stress–strain behavior of the three Butvars plasticized at 32 parts per hundred (phr) varies considerably as well, although T_gs for the three materials, as well as thermal conductivities, do not vary (Table III, last three columns).

The low-frequency microscopic chain motions monitored by $\langle T_{1\rho}(C)\rangle$ and $\langle T_{1\rho}(H)\rangle$ show the same trend with plasticizer concentration as the modulus and T_g for polymer A (Table III, rows 1–4). All $\langle T_{1\rho}(C)\rangle$'s have weak H_1(C) dependences (Table IV) with those for fully plasticized Butvar (32 phr) about nil. The $T_{1\rho}$s are sufficiently short for the plasticized material that motion can make a significant contribution to line widths, accounting, in part, for the observed poor resolution. The high-frequency motions monitored by $\langle T_1(C)\rangle$ and thermal conductivity are independent of plasticizer concentration (Table III, columns 4 and 8).

Dipolar-echo refocusing also decreases with plasticizer from 64% (0 phr) to 44% (32 phr) (Table III, column 6). These values describe the fraction of ^{13}C magnetization that echoes after one rotor period (16 cycles) of multiple-pulse proton decoupling. In the dipolar rotational spin-echo experiment, the percentage of refocusing is the ratio of the signal intensity observed following one rotor period of MREV-8 decoupling to that following a rotor period of dipolar decoupling.[11] Standard refocusing for a typical organic crystal was 75%. Dimunition in refocusing is often attributed to interferences with homonuclear decoupling by molecular motion.[28]

Amplitudes of Motion and Dipolar Sideband Patterns. The decrease in relative $\langle T_{1\rho}(C)\rangle$'s for butyral resin

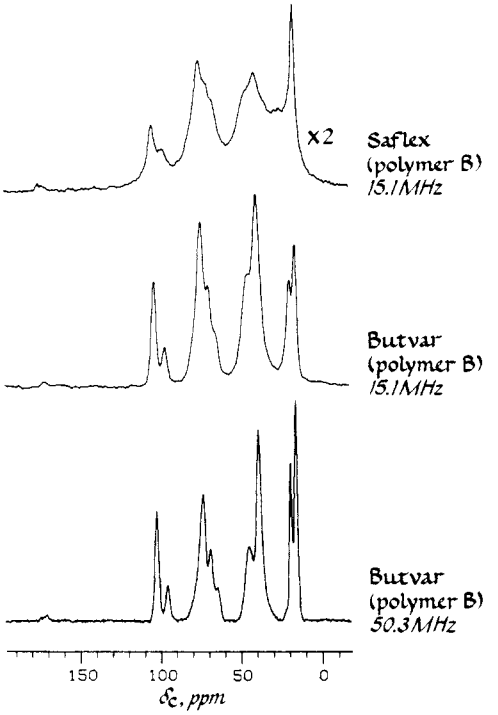

Figure 4. Comparisons of CP MAS ^{13}C NMR spectra of a Butvar resin (polymer B) with (top) and without (middle) plasticizer, the latter at two Larmor frequencies (middle and bottom). The similarity of the low- and high-field spectra indicates that line widths for the unplasticized resin are determined primarily by isotropic chemical-shift disperisons.

main chains with increasing plasticizer, together with the decrease in H_1(C) dependence (Table IV), mean that the mid-kilohertz regime motions to which $T_{1\rho}(C)$'s are sensitive are changing in frequency with plasticizer concentration. However, the insensitivity of the dipolar rotational sideband pattern to plasticizer (Figure 5) shows that these motions are not changing significantly in amplitude. Butvar and plasticized Butvar resin in regions detected by CP MAS have CH dipolar patterns for the butyral units (Table V, 103, 75, and 67 ppm lines) that show total rotational reorientation of no more than about 10° (rms) (Table V, row 10).

The C–H dipolar patterns for the vinyl alcohol units in unplasticized Butvar (Table V, 61 ppm line, row 8) show rotational motion for those units similar to that of the butyrals. The pattern for vinyl alcohol units in plasticized Butvar (Table V, 61 ppm line, row 4) is complicated by a significant centerband (although minor first sideband) contribution from plasticizer carbons with a resonance near 60 ppm (Figure 3). Even though the plasticizer is suffi-

Table V
Dipolar Rotational Sideband Intensities[a] for a CH Pair Undergoing Molecular Motion and Magic-Angle Spinning at 1859 Hz

experiment or motional model	sideband no. 0	1	2	3	4	5	6
Butvar (polymer A) plus 32 phr plasticizer							
103 ppm line	0.123	0.121	0.167	0.082	0.043	0.022	0.004
75 ppm line	0.159	0.121	0.149	0.085	0.041	0.020	0.004
67 ppm line	0.129	0.129	0.151	0.088	0.043	0.018	0.004
61 ppm line	0.311	0.099	0.120	0.067	0.037	0.023	0.000
Butvar (polymer A)							
103 ppm line	0.124	0.124	0.168	0.086	0.040	0.015	0.004
75 ppm line	0.128	0.128	0.156	0.087	0.044	0.017	0.003
67 ppm line	0.130	0.130	0.150	0.083	0.044	0.019	0.004
61 ppm line	0.135	0.136	0.144	0.086	0.045	0.018	0.003
static[b]	0.124	0.133	0.185	0.070	0.034	0.012	0.004
wiggles (10° rms CH reorientation on a sphere)	0.130	0.146	0.182	0.064	0.030	0.009	0.003

[a] Semiwindowless MREV = 8 multiple-pulse decoupling. Theoretical scale factor is 0.54. [b] Effective scale factor (see ref 11) is 0.39.

Table VI
Sphere-Model Fit to Small-Angle Neutron Scattering for Three Plasticized Butvar Resins

polymer	plasticizer concn, phr	$(\delta\rho)^2 \times 10^{18}$,[a] cm^{-4}	R, Å	Q, $\times 10^{17}$ cm^{-4}	Δ^2[b]
A	0	2.84	561	3.23	0.86
	10	2.85	430	4.05	0.88
	20	2.88	450	3.98	0.86
	32	4.25	407	6.10	0.91
B	32	3.45	480	4.62	0.86
C	32	2.81	310	4.40	0.73

[a] $\delta\rho$ is the difference between ρ and the scattering-length density of the matrix within which the spheres are imbedded. [b] $\Delta^2 = (\sum_{k=1}^{N}(I_k(\text{calcd}) - I(\text{av}))^2)/(\sum_{k=1}^{N}(I_k(\text{obsd}) - I(\text{av}))^2)$, where $I(\text{av}) = \sum_{k=1}^{N} I_k(\text{obsd})/N$, and N is the total number of absolute scattering intensities in the data set summed over all k scattering vectors.

ciently immobilized that it reports in a cross-polarization experiment, C–H dipolar couplings are relatively weak because of fast large-amplitude motions.[22] Nevertheless, the vinyl alcohol units of plasticized Butvar can be judged not to be undergoing increased-amplitude motions due to plasticizer because the n_2/n_1 dipolar-sideband ratio is still close to the 1.2 value of Butvar itself.

Small-Angle Neutron Scattering. Unplasticized Butvar resin has a natural contrast, giving rise to a SANS pattern that can be reasonably fit by a spherical scattering function (Table VI, row 1). The scattering contrast arises from regions of differing composition, which for chains packed in the glass means local concentrations of one of the comonomers over the other, within a domain large enough to scatter. The simple, spherical scattering model suggests a domain radius of about 500 Å. This is large enough to scatter neutrons but not large enough to scatter light, consistent with the clear appearance of the molded resin. The neutron scattering contrast increases linearly with plasticizer concentration but the spherical domain size remains the same (Table VI, rows 2–4). This result means an accumulation of plasticizer within the spherical domains or in the matrix surrounding the spherical domains, with either possibility leading to an enhanced scattering contrast. The quality of the fit of the observed absolute scattering intensity by the sphere model (as measured by Δ^2, Table VI, column 6) is only fair and can be improved by invoking a structured spherical scattering function. This model consists of an inner sphere of one scattering density surrounded by a spherical shell of another scattering density. Within this model, the inner core shrinks with increasing plasticizer concentration as its scattering density increases (Table VII, rows 1–4). Figure 6 shows a comparison of the quality of the fit of the absolute scattering intensity as a function of scattering vector by the simple sphere and spherical shell-core models. The scattering invariant, Q, is fit by the shell-core spherical scattering function to within the 95% statistical confidence

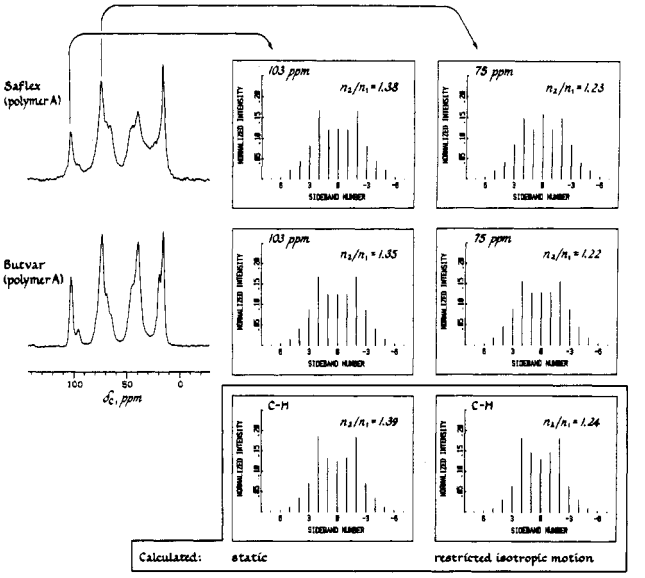

Figure 5. 15.1-MHz CP MAS ^{13}C dipolar rotational spin-echo spectra (after zero MREV-8 decoupling loops) for a Butvar resin (polymer A) with 32 phr plasticizer (top left), and without plasticizer (bottom left). Experimental dipolar rotational sideband patterns for two lines for each polymer system are shown at the right (top and middle) and compared to calculated patterns under two assumptions about molecular motion (bottom).

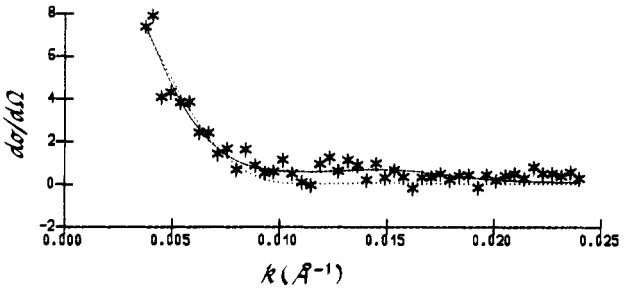

Figure 6. Radially averaged absolute SANS intensity as a function of scattering vector, k, for a Butvar resin (polymer A) with 32 phr plasticizer. Coherent- and incoherent-background scattering have been subtracted. Calculated intensity for scattering from spheres is shown by the dotted line and that from spherical shell-core structures by the dashed line.

levels for all the Butvar and Saflex systems, except for plasticized Butvar polymer C (Figure 7).

Discussion

Composition and Partitioning. The results of Figure 3 show that both liquidlike and solidlike regions are present in plasticized Butvar resins. The former are detected by FT MAS and the latter by CP MAS ^{13}C NMR. Some polymer is almost in solution in the plasticizer since the broad component centered at 60 ppm in the FT MAS spectrum of the plasticized resin has increased in intensity

Table VII
Shell-Core Sphere-Model Fit to Small-Angle Neutron Scattering for Three Plasticized Butvar Resins

polymer	plasticizer concn, phr	$\delta\rho_1 \times 10^{10}$,[a] cm^{-2}	R_1, Å	$\delta\rho_2 \times 10^{10}$,[b] cm^{-2}	R_2, Å	R_2/R_1	$Q \times 10^{17}$, cm^{-4}	Δ^2[c]
A	0	0.65	534	0.08	1263	2.37	4.32	0.90
	10	1.39	210	0.08	635	3.02	7.56	0.90
	20	2.19	152	0.09	597	3.93	10.9	0.88
	32	3.16	140	0.09	574	4.10	20.5	0.95
B	32	2.60	155	0.08	663	4.28	15.2	0.89
C	32	2.84	134	0.06	501	3.74	11.9	0.79

[a] $\delta\rho_1 = \rho_1 - \rho_2$. [b] $\delta\rho_2$ is the difference between ρ_2 and the scattering-length density of the matrix within which the spheres are imbedded. [c] Δ^2 is defined in footnote b, Table VI. A value of Δ^2 close to 1 indicates a good fit of the observed scattering intensities to those calculated for the model.

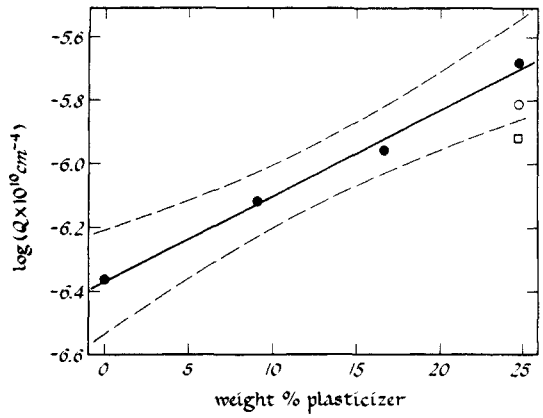

Figure 7. log of the SANS invariant, Q, for plasticized Butvar resins as a function of plasticizer concentration: filled circle, polymer A; open circle, polymer B; open square, polymer C. The least-squares fit to the data for polymer A is shown by the solid line, with the 95% confidence level indicated by the dotted line. A shell-core sphere model was used to obtain Q.

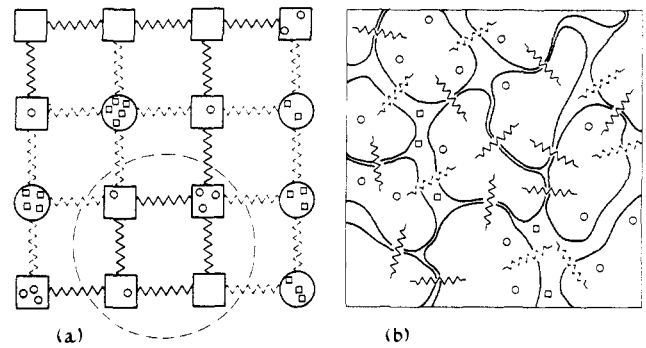

Figure 8. Two stylized representations of the partitioning of Butvar resin and dihexyl adipate plasticizer in Saflex. Both representations are two-dimensional slices through the solid. On the left (a), squares represent polymer and circles, plasticizer. Small circles within large squares represent immobilized plasticizer, and small squares within large circles, dissolved polymer. The size of the large square is that of the intrinsic motional unit capable of kilohertz-regime main-chain motion and is defined by one to a few monomer repeats down a single chain and perhaps a few similarly sized units on neighboring chains. The coupling between units depends on plasticizer. Several coupled squares form a polymer bundle, an example of which is shown within the dashed boundary. On the right (b), the steric constraints on tightly packed motional units are revealed.

compared to that of the CP MAS spectrum. Apparently, this polymer fraction is not quite undergoing full isotropic motion (with correlation times much less than the inverse of the proton-decoupling frequency) since the polymer resonance is poorly resolved.[29] Most of the resin remains in the solid state, based on relative intensities of CP and FT spectra. In addition, some plasticizer is almost in the solid state. Dipolar coupling is sufficient for at least the protonated carbons of this immobilized fraction to be cross polarized. This fraction does not contribute to the broad, unresolved line in the FT MAS spectrum because that line is centered near 60 ppm, which is close to the center of the spectrum for the polymer but not for the plasticizer.

The poly(vinyl alcohol) to polybutyral compositional ratio of the polymer that has gone into solution is not much different from that of the polymer remaining in the solid state. This conclusion is based on the relative Butvar and Saflex CP MAS intensities of the lines centered at 100 and 40 ppm, respectively (Figure 3, lower left and lower right). The ratios of integrated intensities are about the same in the two spectra. Since poly(vinyl alcohol) carbons contribute to the line at 40 ppm but not to the line at 100 ppm, compositional fractionation would have resulted in unequal ratios.

The partitioning of polymer and dihexyl adipate between soft and hard regions was established for the three Butvar resins, one of them as a function of plasticizer concentration (Table II). The three fully plasticized resins have different local compositions despite having the same average composition. Plasticized Butvar polymer B, for example, has significantly more dihexyl adipate immobilized and less polymer in solution than either plasticized polymers A or C (Table II, last two columns). Polymer C has the most signal intensity not accounted for by either the FT MAS or CP MAS spectra (Table II, fifth column). We attribute this loss of signal to mobile polymer not yet in solution but with rotational reorientation comparable to the dipolar-decoupling frequency and hence not observable in the CP MAS experiment. Even without this lost fraction, polymer C has the largest percentage of resin in solution of the three fully plasticized Butvars (Table II, last column).

The decreased ratio of β to α components of the anomeric carbon resonance for polymer A without plasticizer (Figure 2), compared to that of polymer B (Figure 4, bottom), indicates a difference in local structure of the ring on quenching to the glassy state for those two resins. Similarly, we attribute variations in the β/α ratio in the presence of dihexyl adipate (Table II, column 7, rows 1–4) to variations in local solvation of structurally heterogeneous main chains by the plasticizer.

Model of Plasticization of Butvar Resin. The partitioning of plasticizer and polymer between hard and soft fractions in Saflex, reported in Table II for a particular Butvar resin (polymer A), can be represented schematically (Figure 8, left). Here, squares represent polymer and circles, plasticizer. Small circles within large squares represent immobilized plasticizer and small squares within large circles dissolved polymer. After some critical level of circles builds up within a square, the picture changes to a circle containing squares.

Some of the molecular dynamics summarized in Table III (first four rows) can be interpreted within this scheme. The ultrahigh-frequency ps duration bond and atomic-site motions responsible for thermal conductivity[30] are unaffected by diluent within the polymer since both have about the same density. Similarly, the local motions responsible for average T_1 spin–lattice relaxation of the solid polymer (that fraction detected in the CP experiment) are also insensitive to the presence of a few immobilized diluent molecules.[31] These motions occur entirely within the large squares shown in Figure 6 (left).

We imagine each of the large squares to consist of one to a few monomer repeats down a single chain and similarly sized groups on a few neighboring chains.[32] These units are then some 50–100 Å in diameter. The slow motions monitored by $T_{1\rho}$s require cooperativity between several of these units. Proximate units under random packing may have locally parallel or nearly parallel segments that can move together with a minimum of interference.[33] These units can then join to form a bundle[34] which is represented in cross section by a collection of adjacent large squares, an example of which is shown inside the dotted boundary in Figure 8 (left). Bundles may be 100–500 Å in diameter.

The SANS results support this sort of model for plasticized Butvar. We identify the neutron-scattering spheres of Table VI with the bundle of Figure 8. As plasticizer is added to Butvar, scattering contrast increases since more solvent accumulates in the large circles of Figure 8 than in the large squares. Despite the structure of this two-

phase system, the average path of any single chain winding through the solid part of the structure is still random, so that all chains maintain their unperturbed end-to-end dimensions in the glass.

The intrabundle motion is characterized by the solid spring in Figure 8. Some of the springs may be complex with viscous character so that in principle some intrabundle motions can be slow. The effect of plasticizer concentration on the low-frequency motions is represented by the altered springs between large squares and circles. The dashed lines indicate looser coupling, permitting increased cooperative kilohertz-regime motion. The $\langle T_{1\rho}(C)\rangle$'s of the plasticized resin are shorter than those of the resin since units that were formerly rigid are now moving. The fact that the $H_1(C)$ dependence of the short $\langle T_{1\rho}(C)\rangle$'s of the plasticized resin is even weaker than that of the resin itself means that the average kilohertz-regime frequency has been increased to well over 100 kHz by the plasticization.

We know from the dipolar patterns of the solid polymer both with and without plasticizer that the *amplitude* of motion is not sensitive to plasticizer concentration. This notion is not obvious in the circle-and-square representation, so we invoke a second representation, which is shown in Figure 8 (right) as a two-dimensional slice through the solid. Here the shapes of the polymer motional units and regions of high plasticizer concentration are represented schematically. Because of the lock-and-key properties of tight packing, altered spring constants can significantly change frequencies but not amplitudes of motions. Rotational reorientation of several motional units can occur, and the increased mass for this correlated motion ensures a low frequency, but the steric contraints of nearby chains restrict the amplitudes of such motions to close to those of the unplasticized polymer.

Comparisons of Fully Plasticized Resins. We attribute the differences in T_1s and $T_{1\rho}$s for polymers A, B, and C (32 phr plasticizer) to differences within the polymer bundles discussed above. For example, differences in the structure of the bundles for the three plasticized resins are evident in differences in the ratios of α and β components of the 103 ppm line (Table II, column 7). These variations are sensitive to the average configuration of butyral rings which, in turn, affects local chain mobility and so T_1s. In addition, even though the average chemical composition of the three resins is the same, details of the molecular weight distribution are not (Table I). Polymer B, for example, has proportionally more chains of long length than either polymers A or C. Thus, local accumulations of poly(vinyl alcohol) units, from either the same or adjacent chains, can be anticipated to vary from one resin to the next. This is true just because it is easier to pack dissimilar parts of different chains together if some of the chains are short and flexible.

Perhaps packing explains the extent of plasticizer immobilized in the solid matrix, the amount of polymer in solution, and the polymer unaccounted for by either CP or FT experiments (Table II, bottom three rows). In any event, in view of the likely variations in distribution of plasticizer, it is not surprising that those intrabundle motions monitored by $T_{1\rho}(C)$'s which depend on couplings influenced by plasticizer are not identical for polymers A, B, and C. So far, however, we have found no way to gain insight into the heterogeneity of the polymer–plasticizer mixture from the $T_{1\rho}$s.

Plasticizer Concentration and Mechanical Properties. The T_g of the Butvar resin has the simple dependence on plasticizer concentration expected for a reasonably compatible polymer–diluent system.[35] But stress relaxation (as monitored by the modulus after 10^4 s under constant torsional strain at 60 °C, Table III, column 7) has no simple dependence on the composition, partitioning, or dynamics summarized in Tables I–III. In other words, the stress relaxation of resins with 32 phr plasticizer is not directly correlated with chain-length distribution (M_z/M_n), with local chain structure (β/α ratio), with the fraction of immobilized plasticizer, with the fraction of solubilized polymer, with local chain mobility ($\langle T_1(C)\rangle$), or, in terms of the model of Figure 8, with intrabundle mobility ($\langle T_{1\rho}(C)\rangle$).

There certainly is no compelling reason to expect a correlation of stress relaxation with compositional parameters. However, we are not surprised by the lack of a correlation with microscopic dynamics either. We have come to the conclusion that important macroscopic mechanical properties such as stress–strain behavior, creep, aging, and impact strength are poorly predicted from dynamics parameters derived exclusively from NMR experiments.[36]

We believe the reason for this situation is that microscopic chain dynamics are necessary but not sufficient conditions for macroscopic motion. We believe that the second-duration period of motions commonly associated with the macroscopic flows leading to stress relaxation involves not *intra*bundle cooperativity but *inter*bundle cooperativity.[32] We suspect that collections of bundles form domains that are incapable of translational or rotational reorientational motion without the fluctuations of intrabundle motions. Nevertheless, because of unfortuitous packing, such thermally activated fluctuations may accommodate no macroscopic motion.

The only NMR parameter of Table III that has a one-to-one correspondence with the stress–relaxation data of the plasticized resin is the extent of refocusing of the rotational dipolar spin echo. The lack of refocusing is a measure of homogeneous proton–proton dipolar interactions characterized by a time constant comparable to that of the multiple-pulse decoupling cycle.[28] We attribute the observed dephasing to proton–proton interactions on the periphery of translating bundles.

It is possible that the motions of bundles that are capable of dephasing the dipolar echo might also indicate the presence of domains properly situated for the reorganization needed for shear flow and stress relaxation. It is also possible that the large outer-shell to inner-core ratio of the shell-core neutron scattering model for plasticized Butvar B (R_2/R_1 = 4.28, Table VII, column 7) reflects the sort of bundle structure needed for flow. That is, an oversized shell that structurally matches the surrounding matrix may facilitate the translation and reorientation of a shell-core bundle.

Acknowledgment. Preliminary CP MAS measurements on Butvar (polymer A) with and without 32 phr plasticizer were performed by J. P. Desmoulins, a student visiting Monsanto, in partial fulfillment of the requirements for the Diplôme d'Etudes Approfondies, École Supèrieure de Physique et de Chimie Industrielles de la Ville de Paris. Molecular weight distributions were characterized by E. E. Remsen (Monsanto, St. Louis). Stress–relaxation data were provided by G. Matis (Monsanto, Indian Ordhard, MA) and thermal conductivity data by A. J. Brezinski (Dynatech Thermophysics Laboratory, Cambridge, MA). Assistance in performing the SANS experiments was provided by Dr. J. M. Fuller (University of Massachusetts Chemical Engineering Department) and in interpreting SANS data by Dr. G. D. Wignall (Oak

Ridge National Laboratory).

Registry No. Dihexyl adipate, 110-33-8; neutron, 12586-31-1.

References and Notes

(1) Bernardo, J. J.; Burrell, H. In *Polymer Science*; Jenkins, A. D., E.; North-Holland: Amsterdam, 1972; Vol 1, p 537.
(2) Ferry, J. D. *Viscoelastic Properties of Polymers*; Wiley: New York, 1980; p 486.
(3) Nielsen, L. E. *Mechanical Properties of Polymers*; Reinhold: New York, 1962; p 168.
(4) Theodorou, M.; Jasse, B. *J. Polym. Sci., Polym. Phys. Ed.* **1983**, *21*, 2263.
(5) Schaefer, J.; Stejskal, E. O. *Top. Carbon-13 NMR Spectrosc.* **1979**, *3*, 384.
(6) Eckman, R.; Alla, M.; Pines, A. *J. Magn. Reson.* **1980**, *41*, 440.
(7) Doty, F. D.; Ellis, P. D. *Rev. Sci. Instrum.* **1981**, *52*, 1868.
(8) Stejskal, E. O. U.S. Patent 4 446 430, May 1, 1984.
(9) Stejskal, E. O.; Schaefer, J.; Steger, T. R. *Faraday Symp. Chem. Soc.* **1978**, *13*, 56.
(10) Schaefer, J.; Sefcik, M. D.; Stejskal, E. O.; McKay, R. A. *Macromolecules* **1984**, *17*, 1118.
(11) Schaefer, J.; McKay, R. A.; Stejskal, E. O.; Dixon, W. T. *J. Magn. Reson.* **1983**, *52*, 123.
(12) Hester, R. K.; Ackerman, J. L.; Neff, B. L.; Waugh, J. S. *Phys. Rev. Lett.* **1976**, *36*, 1081.
(13) Stoll, M. E.; Vega, A. J.; Vaughan, R. W. *J. Chem. Phys.* **1976**, *65*, 4093.
(14) Waugh, J. S.; Huber, L. M.; Haeberlen, U. *Phys. Rev. Lett.* **1968**, *20*, 180.
(15) Munowitz, M. G.; Griffin, R. G.; Bodenhausen, G.; Huang, T. H. *J. Am. Chem. Soc.* **1981**, *103*, 2529.
(16) Munowitz, M. G.; Griffin, R. G. *J. Chem. Phys.* **1982**, *76*, 2848.
(17) Mansfield, P.; Orchard, M. J.; Stalker, D. C.; Richards, K. H. B. *Phys. Rev.* **1973**, *37*, 90.
(18) Rhim, W. K.; Elleman, D. D.; Vaughan, R. W. *J. Chem. Phys.* **1973**, *59*, 3740.
(19) Burum, D. P.; Linder, M.; Ernst, R. R. *J. Magn. Reson.* **1981**, *44*, 173.
(20) Spiess, H. W. *Colloid Polym. Sci.* **1983**, *261*, 193.
(21) Herzfeld, J.; Berger, A. E. *J. Chem. Phys.* **1980**, *73*, 6021.
(22) Schaefer, J.; Stejskal, E. O.; McKay, R. A.; Dixon, W. T. *Macromolecules* **1984**, *17*, 1479.
(23) Wignall, G. D.; Child, H. R.; Samuels, R. J. *Polymer* **1982**, *23*, 957.
(24) Hayashi, H.; Flory, P. J.; Wignall, G. D. *Macromolecules* **1983**, *16*, 1328.
(25) Cooper, S. L.; Yarusso, D. J. *Macromolecules* **1983**, *16*, 1871.
(26) Higgins, J. S.; Stein, R. S. *J. Applied Crystallogr.* **1978**, *11*, 346.
(27) Maciel, G. E.; Kolodziejski, M. S.; Bertran, M. S.; Dale, B. E. *Macromolecules* **1982**, *15*, 686.
(28) Haeberlen, U.; Waugh, J. S. *Phys. Rev.* **1968**, *175*, 453.
(29) Pines, A.; Gibby, M. G.; Waugh, J. S. *J. Chem. Phys.* **1973**, *59*, 569.
(30) Van Krevelen, D. W. *Properties of Polymers*; Elsevier: New York, 1976; p 395.
(31) Edzes, H. T.; Veeman, W. S. *Polym. Bull. (Berlin)* **1981**, *5*, 255.
(32) Skolnick, J.; Perchak, D.; Yaris, R. ; Schaefer, J. *Macromolecules* **1984**, *17*, 2332.
(33) Schaefer, J.; Stejskal, E. O.; Perchak, D.; Skolnick, J.; Yaris, R. *Macromolecules* **1985**, *18*, 368.
(34) Volkenstein, M. V. *Configurational Statistics of Polymeric Chains*; Interscience: New York, 1963; pp 546–552.
(35) Bueche, F. *Physical Properties of Polymers*; Interscience, New York, 1962; p 116.
(36) Steger, T. R.; Schaefer, J.; Stejskal, E. O.; McKay, R. A. *Macromolecules* **1980**, *13*, 1127.

Inverse Gas Chromatography. 4. The Diffusion Phenomena on the Column

Petr Munk,* Timothy W. Card, Paul Hattam, Mohammad J. El-Hibri, and Zeki Y. Al-Saigh

Department of Chemistry and Center for Polymer Research, University of Texas at Austin, Austin, Texas 78712. *Received August 22, 1986*

ABSTRACT: Broadening of chromatographic peaks in inverse gas chromatography experiments was analyzed. An evaluation technique was designed, allowing calculation of gas–gas mutual diffusion coefficients of a number of probes at a number of temperatures, provided that this coefficient is known for a single probe at a single temperature from an independent experiment. Under a similar condition, mutual diffusion coefficients of various probes in amorphous polymers above the glass transition temperature may be measured at a number of temperatures. The method yielded a dependence of the diffusion volume of normal alkanes in the gas phase on the chain length. The diffusion constants of normal alkanes in polyisobutylene at a number of temperatures were also obtained.

Introduction

Diffusion processes on gas chromatographic columns lead to broadening of the chromatographic peak. In traditional gas chromatography, the peak broadening is directly related to the resolving power of the columns and as such has received extensive theoretical interest.[1,2] There are two major factors that contribute to peak broadening: diffusion of the injected compound (probe) in the carrier gas and diffusion of the probe in the stationary phase. The former factor is characterized by the gas-phase mutual diffusion coefficient, D_g, and the latter factor is related to the liquid-phase mutual diffusion coefficient, D_L.

In the case of inverse gas chromatography (IGC) experiments, where a polymer is the stationary phase, D_L is a polymer-probe diffusion coefficient, an interesting quantity both experimentally and theoretically. Gray and Guillet[3] were able to measure the D_L coefficients of a small number of probes using as their stationary phase, low-density polyethylene coated onto glass beads. Miltz[4] investigated the diffusion of styrene in polystyrene at various temperatures using polystyrene coated onto Chromosorb P as the stationary phase.

During our recent IGC investigations we accumulated a large body of data using polyisobutylene (PIB) coated onto Chromosorb W as the stationary phase and linear alkanes from methane to undecane as probes. In the experiments, temperature, flow rate of carrier gas, and column loading were varied systematically. We have also designed a method of evaluating peak-broadening data from which both diffusion coefficients, D_g and D_L, may be obtained. The purpose of this paper is to determine the quality of the acquired data and the amount of information that may be extracted from them.

Theory

We will follow the standard chromatographic approach in expressing the distribution of a probe on the column by means of the height equivalent to one theoretical plate

0024-9297/87/2220-1278$01.50/0